



The Amyloid Precursor Protein Shows a pH-Dependent Conformational Switch in Its E1 Domain

Sandra Hoefgen, Sven O. Dahms, Kathrin Oertwig and Manuel E. Than

Protein Crystallography Group, Leibniz Institute for Age Research, Fritz Lipmann Institute (FLI), Beutenbergstrasse 11, 07745 Jena, Germany

Correspondence to Manuel E. Than: than@fli-leibniz.de, http://www.fli-leibniz.de/groups/than_en.php
<http://dx.doi.org/10.1016/j.jmb.2014.12.005>

Edited by J. Bowie

Abstract

The amyloid precursor protein (APP) and its proteolytic cleavage product A β are widely believed to be central to the etiology of Alzheimer's disease (AD). APP and its family members are also essential for proper neuronal development and homeostasis. APP is located at the cell surface and within intracellular compartments, cellular regions that exhibit different pH values. The AD-associated amyloidogenic processing of APP is initiated predominantly in intracellular acidic compartments, whereas its non-amyloidogenic cleavage is initiated at the cell surface at slightly basic pH. We analyzed the influence of pH on the APP-E1 domain and found that its two constituting subdomains, GFLD and CuBD, interact with each other in a pH-dependent manner. Dynamic light scattering showed that APP-E1 represents a more open conformation at neutral pH and a more closed conformation at acidic pH. Analyzing a 1.4 Å, high-resolution X-ray structure of E1 derived from merohedrally twinned crystals resulted in the identification of individual residues that are responsible for these pH-dependent interactions. Mutational studies and dynamic light scattering measurements further proved that specific hydrogen bonds between the two carboxylates of D177 and E87, as well as between N89 and H147, are major determinants of this pH-driven conformational switch in APP-E1. These findings show how APP can adopt different conformations depending on pH and suggest that the protein fulfils different functions at distinct localizations within the cell. Additionally, our data suggest a novel strategy for treating AD based on regulating the amyloidogenic processing of APP by the specific interruption of the interaction between the APP-E1 subdomains.

© 2014 The Authors. Published by Elsevier Ltd. This is an open access article under the CC BY-NC-ND license (<http://creativecommons.org/licenses/by/3.0/>).

Introduction

The type I transmembrane protein amyloid precursor protein (APP) and its proteolytic processing to the neurotoxic A β peptide are generally believed to be central to the etiology of Alzheimer's disease (AD). APP is cleaved in two alternative pathways either by α - and γ -secretase into the non-toxic fragments sAPP α , p3 and the intracellular domain (AICD) or by β - and γ -secretase into sAPP β , the neurotoxic A β peptide and AICD (e.g., reviewed in Refs. [1–3]). In addition, various physiological functions are described for APP including synaptic outgrowth [4], metal binding and transport [5,6], regulation of gene transcription [7,8], cell–cell interaction [9,10] or a receptor function [11]. Thus, APP also has an essential physiologic function related to neuronal development and activity, although

its exact cellular role and that of its two homologues, the APP-like protein 1 (APLP1) and APP-like protein 2 (APLP2), remains to be established.

APP travels as a typical type I transmembrane protein during biosynthesis through the constitutive pathway to the cell surface. Here it is also re-internalized and transported to the lysosomal pathway or again recycled into the secretory pathway (e.g., reviewed in Ref. [12]). The cellular compartments largely differ in their pH value, which typically is slightly basic at the cell surface (pH ~7.4), slightly acidic (pH ~6.5–5.5) within the secretory pathway and more acidic in endosomes (pH ~5.7) or lysosomes (pH ~5.0) [13,14]. Interestingly, the proteolytic processing of APP is different at distinct parts of the cell: the β -secretase is predominantly active within the lysosomal compartments and produces neurotoxic proteolysis fragments. The

non-amyloidogenic processing of APP, however, is initiated by α -secretase at the cell surface [2,15]. Thus, the subcellular localization of APP has an influence on its proteolytic processing and hence the generation of the neurotoxic A β . As the subcellular location of α - and β -secretase differs markedly in pH, this raises also the question whether the different pH values affect the structure of APP and with that its susceptibility to processing by either α - or β -secretase. Interestingly, not only the generation of A β but also its aggregation seems to be pH dependent [16]. It could also be shown that lowering the pH does influence the binding of A β to heparan sulfate proteoglycans [17].

Over the last years, considerable progress in our understanding of the structure of individual domains of APP, their interaction within the entire protein and their relation to certain physiologic functions of this protein has been made (e.g., reviewed in Ref. [18]). Its large ectodomain consists of the two rigidly folded segments E1 [19] and E2 [6,20,21] that are connected to one another and to the transmembrane helix of APP by flexible segments called the acidic domain and the juxtamembrane region, respectively [22]. In turn, E1 consists of the subdomains growth factor like (GFLD) and copper binding domain (CuBD). They were initially described as individual entities at neutral to slightly basic pH values between 7 and 8 [23–25]. Interestingly, these two constituent subdomains tightly interact with each other specifically at the acidic pH of 5.0, now forming one structural and functional unit, the E1 domain [19]. Interestingly, altered pH resulted also in different interaction mode between APP-E1 and heparin in isothermal titration calorimetry experiments [19].

To understand the pH-dependent behavior of the APP-E1 domain, we analyzed its molecular shape at different pH values by dynamic light scattering (DLS) measurements and determined a highly resolved crystal structure of this domain at 1.4 Å in a new crystal form. We identified the responsible pH sensor in APP-E1 by careful analysis of the high-resolution structure and by comparative analyses of the apparent molecular weight of wild-type (wt) E1 and specific E1 mutants in solution. This mechanism might represent a novel target to specifically interfere with A β generation and hence potentially with the development of AD.

Results

Trigonal APP-E1 crystals are almost perfectly twinned

We expressed APP-E1 in *Escherichia coli* Origami B (DE3), purified it to homogeneity using a three-step purification protocol including His-tag cleavage (Fig. S1) and used the respective protein for crystal-

lization. We identified a new crystal form, which resulted from a low-salt condition and diffracted to a resolution of 1.4 Å. The data were merohedrally twinned and the structure was solved by molecular replacement (MR) using the entire E1 domain (PDB ID: 3ktm [19]) as search model revealing two molecules in the asymmetric unit (final Z-score of 29.4, LLG value of 1960.5 and R/R_{free} of 45%/44%).

We refined the structure under consideration of the found twinning operation ($-h, -k, l$) and always used detwinned data for the calculation of electron density maps. In addition, we checked for potential model bias by calculating different omit maps (e.g., see Fig. S2a), which always showed the electron density for the omitted amino acids. The final model was built in ~40 cycles of manual model building completing also the loop between V47 and G50 of both molecules in the asymmetric unit and the heparin binding loop in molecule A (named according to PDB file nomenclature). The latter section of molecule B became not visible in the electron density map, indicating high flexibility of this region. Refinement was finished showing good R -factors, stereochemistry and electron density (Table 1 and Fig. S2b).

Overall structure of APP-E1 at high resolution

The overall fold of the E1 domain is very similar to the previously described entire E1 domain (PDB ID: 3ktm [19]) (rmsd of 0.80 Å, calculated for all C $^{\alpha}$ atoms)

Table 1. Data collection and refinement statistics

<i>Data collection statistics</i>	
Unit cell parameters (Å)	
<i>a</i>	91.4
<i>b</i>	91.4
<i>c</i>	80.0
Resolution range (Å) ^a	50–1.40 (1.47–1.40)
No. of reflections/unique reflections	357,235/70,655
Completeness (%) ^a	98.8 (97.7)
$\langle I/\sigma(I) \rangle$ ^a	16.8 (3.5)
R_{meas} (%) ^{a,b}	6.5 (47.3)
Multiplicity ^a	5.1 (4.9)
<i>Refinement statistics</i>	
Resolution range (Å)	45.70–1.40 (1.4388–1.4151)
No. of reflections	75,220
Atoms protein/water	2519/626
$R_{\text{work}}/R_{\text{free}}$ (%) ^a	15.6/18.6 (22.1/22.1)
Twin fraction	0.49
<i>B</i> -factors overall/protein/water/ Wilson plot (Å ²)	15.7/14.6/20.3/19.8
Ramachandran plot (%) ^c	89.1/10.6/0.4/0
rmsd values of bond length (Å)/ bonded <i>B</i> values (Å ²)	0.007/1.163

^a Values given in parentheses represent the highest-resolution shell. The values for the highest-resolution shell upon refinement are given as provided by the Phenix output.

^b $R_{\text{meas}} = \sum_{hkl} [N(N-1)]^{1/2} \sum_i |I(hkl)_i| - (I(hkl)/\sum_{hkl} \sum_i |I(hkl)_i|)$.

^c Percentage of residues in most favored/additional allowed/generously allowed/disallowed regions of the Ramachandran plot.

(Fig. 1). The higher resolution of 1.4 Å (as compared to 2.7 Å for PDB ID: 3ktm [19]) does, however, allow a much more detailed analysis of individual residues and atoms than previously possible.

The high similarity also extends to the linker region and to the molecular contacts between GFLD and CuBD. The highly resolved E1 structure now clearly shows the importance of individual amino acids for the interaction of both subdomains. They contact each other *via* a central hydrophobic core, the previously identified salt bridge between D125 and R116, several hydrogen bonds and additional polar and water-mediated interactions. The largest differences between the rhombohedral APP-E1 crystals (PDB ID: 3ktm [19]) and the herein determined trigonal APP-E1 structure is found for the heparin binding loop encompassing the segment between C98 and C105 (Fig. 1). This section also shows the highest *B*-factors of the entire E1 domain. Thus, this section is characterized by a general tendency toward flexibility. In order to test for similar structures within the PDB, we compared the two subdomains of E1 to all structurally known proteins within a PDBeFold search [26]. Interestingly, our search identified only the structures of the individually determined GFLD (PDB ID: 1mwp [23]; rmsd of 0.8 Å) and the different CuBDs (PDB IDs: 2fjz, 2fk1, 2fk2, 2fk3 and 2fma [25,27]; rmsd of 0.52–0.91 Å) of APP-E1 and APL-1 (PDB ID: 2m05; rmsd of 1.2 Å [28]), indicating that both subdomains form rather unique folds and are structurally not similar to other known proteins.

We asked next if the previously determined dimeric arrangement of APP-E1 [19] is present in the new crystal form. Alternatively, the herein described trigonal crystals might offer a different explanation for the biochemically observed E1 dimerization by short heparin chains [29]. To check for potential dimeric

arrangements, we analyzed interaction interfaces using the PISA server [30] and identified exclusively interfaces typical for weak molecular contacts usually representing physiologically non-significant crystal contacts (Table S1). None of these interfaces (Fig. S3) contains a continuous, positively charged surface patch as one would expect for a productive dimeric interface that can be stabilized by its interaction with negatively charged heparin molecules. Also none of the observed contacts is in agreement with previously observed amino acid residues and mutations affecting the heparin-induced dimerization of APP-E1 as, for example, residues of the heparin binding loop between C98 and C105 [31] and herein especially K103 and K106 [29]. We thus conclude that the interactions between the different molecules in the trigonal crystal do not represent contacts important for the heparin-induced dimerization of APP-E1. The low ionic strength of our present crystallization condition probably prevents the formation of crystal contacts involving the strongly positively charged loop between C98 and C105 of the GFLD.

pH-dependent apparent molecular weight of APP-E1

Our analysis focused next on the pH-dependent structural and biochemical characteristics of APP-E1. We performed DLS measurements of the E1 domain in dependence of the protein concentration at pH 5.7 and at pH 7.4, corresponding to the pH values of endosomes and of the plasma membrane, respectively (Fig. 2). Independent of pH, we observed an about 2-fold increase of the apparent molecular weight of APP-E1 at high protein concentrations, in accordance with a concentration-dependent dimerization that was described before [29]. In addition, the apparent molecular weight of the APP-E1 domain was

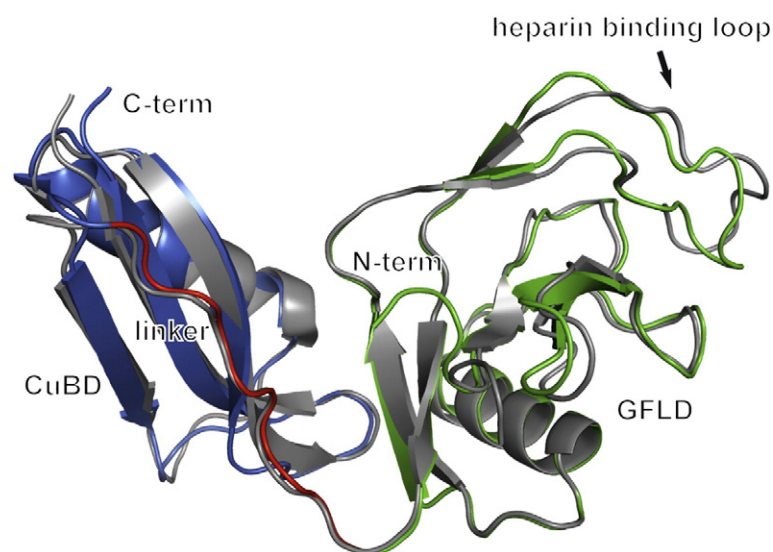


Fig. 1. Overall structure of APP-E1. An alignment of molecule D (named according to PDB file nomenclature) of the replacement model (PDB ID: 3ktm) is shown in gray, with the here described high-resolution structure of APP-E1 depicted for its GFLD in green, the linker region is in red and the CuBD is in blue. Both structures are represented as cartoons and are highly similar. The largest differences can be found in the conformation of the heparin binding loop.

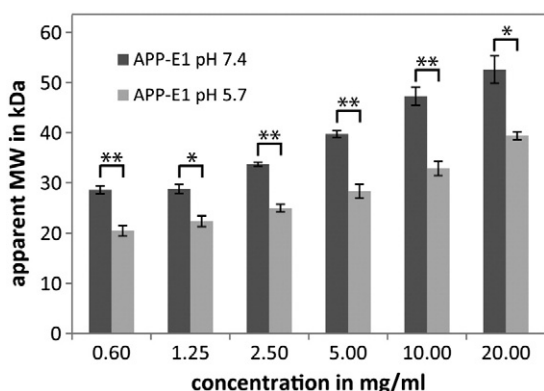


Fig. 2. DLS at different pH values. The apparent molecular weight of APP-E1 was determined by DLS experiments at two different pH values (pH 5.7 and pH 7.4) and at increasing protein concentrations. Averages of three independent experiments \pm standard deviation are shown together with the statistical analysis of the observed differences (* $P < 0.005$, ** $P < 0.001$).

at all protein concentrations significantly lower at pH 5.7 than at pH 7.4. The determination of the apparent molecular weight by DLS is based on the hydrodynamic radius and hence the shape of the analyte. Hereby, the overall shape of the molecule depends on its oligomerization state and on its conformation. Because the observed pH-dependent differences in the apparent molecular weight are seen at all concentrations and hence do not depend on it, one can exclude oligomerization as reason. Accordingly, these data must originate from a more open (and hence a larger hydrodynamic radius) overall conformation at pH 7.4 (representing the cell surface) than observed at the endosomal pH of 5.7.

pH-dependent interaction of GFLD and CuBD

We next analyzed the interface between the GFLD and the CuBD for well-defined interactions (Fig. 3) and compared it to various available structures of APP-E1 subdomains obtained at different pH values (Fig. 4). Interestingly, structures of the whole E1 domain are only available from crystals grown at acidic pH value of 5.0–5.6 and, thus, the formal alignment of the entire E1 domain at different pH is technically not possible. Instead, we superimposed the structures of the two individually solved E1 subdomains onto the entire APP-E1 domain solved in this study. In particular, we used the GFLD (PDB ID: 1mwp [23]) and the CuBD in its ligand-free form (PDB ID: 2fjz [25]) that were both solved at pH values between 7 and 8. In addition, we also superimposed the isolated CuBD solved at acidic pH (PDB ID: 2fk3 [25]), which served as internal control to test for structural effects that solely originate from the crystallization of the isolated subdomain. In principle, found differences could result not only from true pH-induced structural alterations but also from artifacts resulting from different crystal packings. Thus, any such structural comparison can only suggest potential interactions that must be verified by respective mutational analyses later on. In general, the overall fold of both subdomains in isolation is very similar to their structures within the entire E1 domain (Fig S4), which is also shown by the very low rmsd values of the alignments. Comparing the structure of the GFLD (1mwp) solved in isolation at pH 7.5 with the herein shown APP-E1 domain at low pH including amino acids 28–123 resulted in an rmsd value of 0.457 Å. The alignment of the individually solved CuBDs at different pH conditions ranging from 5.4 to 8 with the high-resolution structure of E1 including residues 131–189 showed rmsd values of 0.358 Å

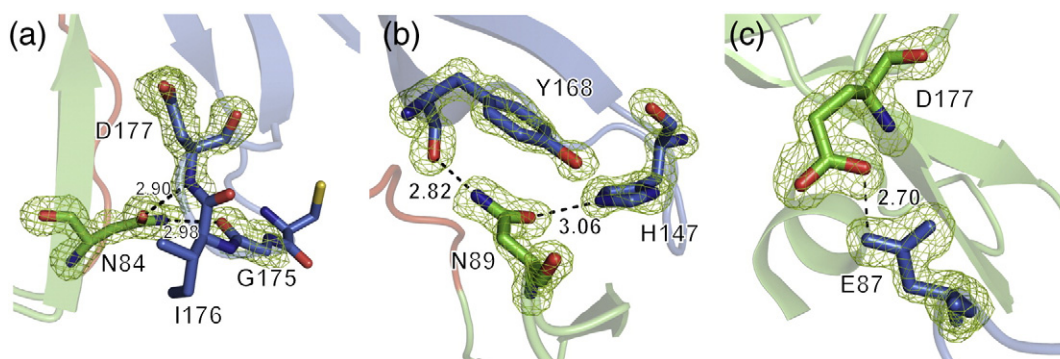


Fig. 3. Distinct pH-dependent interactions at the GFLD–CuBD interface. Analysis of the GFLD–CuBD interface revealed three regions that are formed in a pH-dependent manner. The high-resolution structure of E1 is colored according to Fig. 1 and is shown in a cartoon representation. Interacting residues are depicted as sticks and $F_o - F_c$ omit maps are shown in green and are contoured at 3.0σ for those residues. (a) N84 of the GFLD interacts *via* backbone hydrogen bonds with the CuBD. (b) N89 of the GFLD builds up two hydrogen bonds with H147 and Y168 of the CuBD at acidic pH and therefore connects both subdomains with each other (c) the E87–D177 interaction. Hydrogen bonds are indicated by broken lines and distances are given in angstroms (Å).

and 0.443 Å for 2fjz and 2fk3, respectively. In contrast, the structure of the interface and the contacts between the two subdomains did show major pH-dependent differences.

First, we analyzed the interface areas in between the GFLD and the CuBD at different pH values employing the PISA server [30] to calculate interaction interfaces. The interface area between the subdomains of the herein shown high-resolution E1 structure at pH 5.6 comprised 366 Å². This is very similar to the interface area of the previously obtained E1 structure [19] showing an interface area of 371 Å² (this area is smaller than the originally published value as it had to be recalculated for this study without the contribution of the linker region, which is not present for the individually solved subdomain structures). This interface size is also comparable to the one between the herein shown GFLD (solved at pH 5.6) and the individually solved CuBD structure determined at pH 5.4 (PDB ID: 2fk3), which was calculated to 374 Å². Interestingly, the interaction area decreased by 15–20% to 318 Å² between the two at slightly basic pH individually solved GFLD (pH 7.5) and CuBD (pH 8.0) structures, superimposed onto the entire APP-E1. This reduction in interface area goes along with a reduced number of distinct interactions. Whereas five hydrogen bonds stabilize the interaction at pH 5.6, the same interface does not contain any hydrogen bond if created by superposition with the structures at high pH.

We next analyzed the conformation of the interacting residues in detail in order to understand the observed differences (Figs. 3 and 4). The section responsible for the largest change in interface is a loop of the CuBD encompassing the residues L172–F179, with residues C174–D177 showing the largest conformational changes (Figs. 3a and 4a). Interestingly, also a disulfide bridge is part of these structural alterations. C174 is differently oriented at pH 8.0 compared to pH 5.5/5.6, affecting the conformation of its disulfide linkage to C144. The location of G175 also largely affects the interaction between GFLD and CuBD. A hydrogen bond between this residue (located within the CuBD) and N84 (located within the GFLD) is only present at pH 5.5/5.6 but not at pH 8.0. Furthermore, the residues I176 and D177 of the CuBD are in direct contact with the GFLD only at acidic pH.

The second contact between GFLD and CuBD is formed by the imidazole ring of H147 only acting as hydrogen bond donor to N89 at acidic pH (Fig. 3b). At neutral pH, however, deprotonation of H147 abolishes this interaction. In addition, the side-chain carboxamide nitrogen of N89 forms a hydrogen bond to the main-chain carbonyl oxygen of Y168 (CuBD) and cannot substitute as a possible hydrogen bond donor to a deprotonated H147. Instead, the ring plane of H147 is rotated by ~90° at pH 8.0 now forming an alternative hydrogen bond to the tyrosyl functionality of Y168 (Figs. 3b and 4b). This new

hydrogen bond lies within the CuBD and hence does not stabilize any inter-subdomain contact.

Another interesting contact is formed between E87 of the GFLD and D177 of the CuBD, which face each other directly with their side-chain carboxylates (Figs. 3c and 4c). This conformation is well defined in the 1.4 Å crystal structure of the entire E1 domain at low pH and shows a distance of 2.71 Å between D177-OD2 and E87-OE1. This can only be explained by a pK_a shift and the existence of a tight hydrogen bond between the two carboxylates. Otherwise, the two negatively charged side chains would strongly repel each other. In fact, respective contacts have been studied extensively [32] and the authors describe a pK_a shift of up to ~2.5 pH units. Considering the side-chain pK_a values of aspartate (3.90) and glutamate (4.32), only a moderate shift in pK_a is necessary to form a tight hydrogen bond between the two carboxylates at acidic pH. At higher pH, the two carboxylates are deprotonated and repel each other.

Interestingly, all here described residues (E87, N89, H147, Y168 and D177) are conserved between APP and APLP2 of different vertebrates, but mostly not in vertebrate APLP1 and in the APP homologues of the two model organisms, *Caenorhabditis elegans* and *Drosophila melanogaster* (Fig. S5). This conservation pattern has been noted before [19] and further supports the notion that the interaction between the GFLD and the CuBD within APP-E1 is of functional relevance for vertebrate APP and APLP2, but probably not for APLP1 and evolutionary distant APP homologues.

Mutations in the pH-dependent interface influence the conformational change of E1

Based on our structural investigation, we created specific interface mutants to analyze if the respective residues are truly responsible for the pH-dependent interaction between GFLD and CuBD. In particular, we analyzed the pH-dependent apparent molecular weight of wt-APP-E1, the APP-E1_D177A and APP-E1_N89A mutants (destroying the hydrogen bonds between D177 and E87, as well as between H147 and N89), the double mutant APP-E1_D177A/N89A and the previously described mutant APP-E1_H147N [33] by DLS. The latter mutant is especially interesting as it was shown to affect the trafficking of APP and has been implicated with the binding of Cu²⁺ to the CuBD of E1. Only the wt protein showed hereby the expected pH-dependent difference of apparent molecular weight, corresponding to ~29 kDa at the slightly basic pH of 7.4 and ~20 kDa at the vesicular pH of 5.7 (Fig. 5). All mutants show, in contrast, a largely reduced effect on the apparent molecular weight at the lower pH. Whereas for all mutants, the apparent molecular weight at pH 7.4 is within the experimental error identical with the wt protein, this

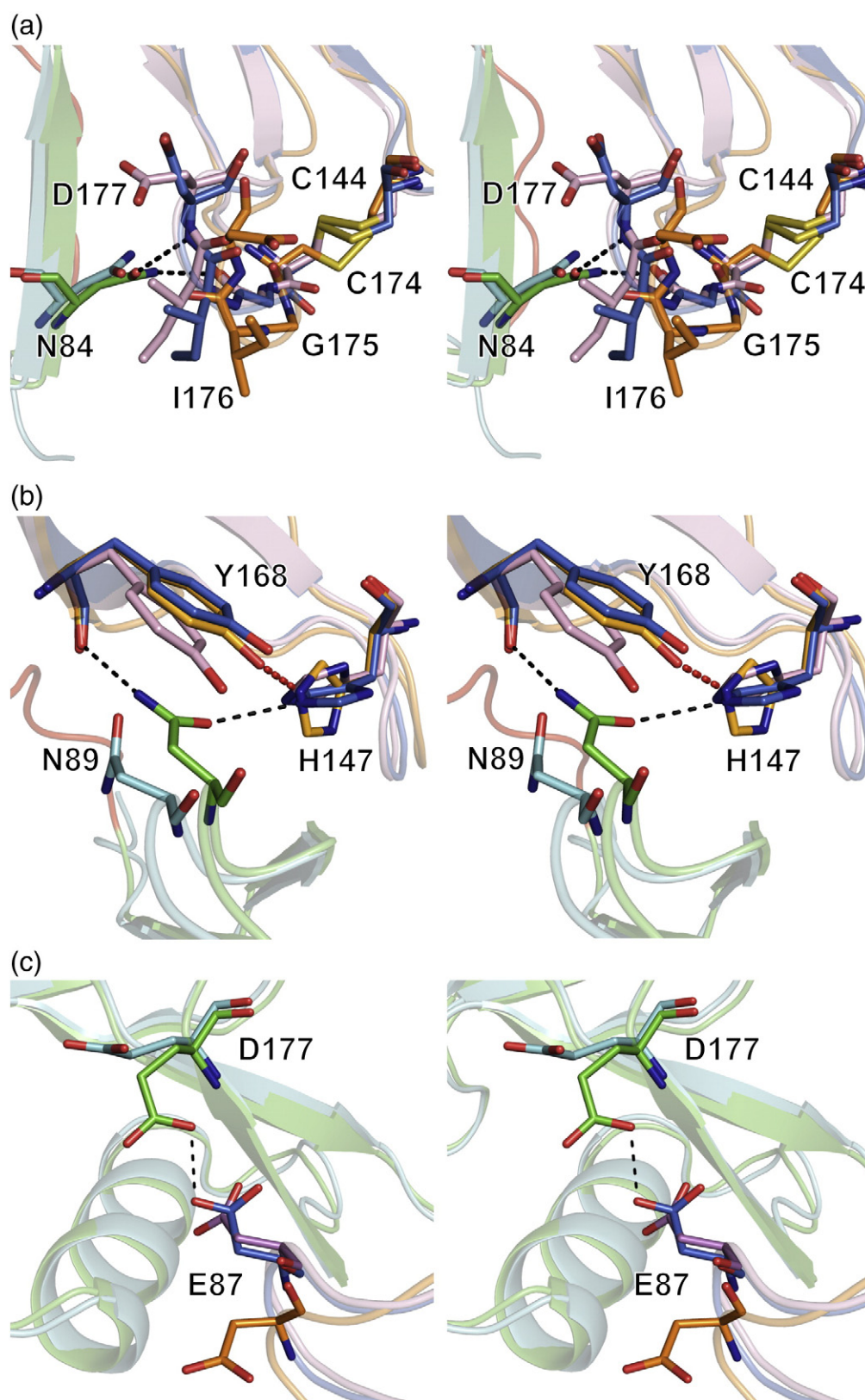


Fig. 4 (legend on next page)

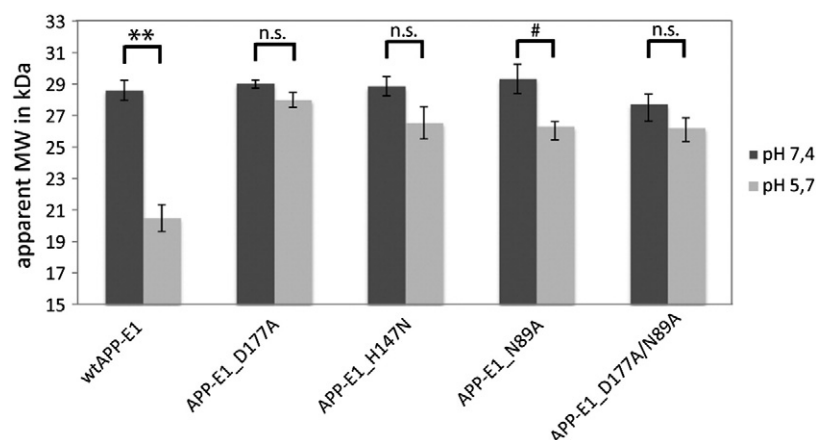


Fig. 5. DLS of different APP-E1 mutants at two pH values. Determination of the apparent molecular weight of APP-E1 and its interface mutants at a concentration of 0.6 mg/ml and at the two different pH values. Whereas wt-APP-E1 showed a roughly 28% difference in the apparent molecular weight at different pH values, basically no such change can be seen within the experimental error for all used mutants. Averages of three independent experiments \pm standard deviation are shown together with the statistical analysis of the observed differences (** $P < 0.001$, n.s. = not significant, # $P = 0.012$).

value is not largely reduced upon lowering the pH (Fig. 5). The observed small differences between the individual mutants, especially for the N89A mutation, might hereby be interpreted as different importance of the respective contact for the pH-dependent interaction. This shows that all mutants are not able anymore to form the specific hydrogen bonds between CuBD and GFLD. Both interactions, the atypical hydrogen bond between the carboxylates of E87 and D177 as well as the hydrogen bond between H147 and N89, are required to stabilize the tight interaction between the two subdomains forming APP-E1 at vesicular pH.

Discussion

The APP is central to neuronal development and the etiology of the neurodegenerative AD. It is located both at the cell surface and within intracellular compartments. Both subcellular localizations differ markedly in their pH, potentially linking different physiological functions or properties of APP to different pH values. Interestingly, a pH-dependent behavior of APP-E1 was already found in solution during limited proteolysis and isothermal titration calorimetry measurements, where the ratio of protein to heparin changed from 2:1 at pH 7.4 to 1:1 at pH 5.7 [19]. To analyze the structural differences of the E1 domain at different pH values, we herein solved the crystal structure of this domain at the

high-resolution limit of 1.4 Å in a new crystal form that turned out to be almost perfectly twinned. Crystals were grown under a low-salt condition, and the structure was determined using MR and refined to good-quality factors. It shows an overall fold similar to the previously determined structure of the entire APP-E1 (PDB ID: 3ktm [19]). The higher resolution allows, however, a detailed analysis of pH-induced conformational changes at the interface between the subdomains GFLD and CuBD that, in addition, were also characterized biochemically.

The presented DLS experiments showed a concentration-dependent self-dimerization of APP-E1 at both pH values that fit nicely to the already characterized heparin-dependent and heparin-independent dimerization of this protein [29]. Interestingly, the apparent molecular weight of the E1 domain is significantly lower at pH 5.7 than at pH 7.4, strongly supporting a more open and flexible conformation of E1 at higher pH as already suggested before [19]. We investigated this aspect in more detail and found by structural and biochemical studies that the total interface area depends on pH. We also identified several key residues that together form a molecular explanation for the observed pH dependence of the interaction between the GFLD and the CuBD within APP-E1. Due to the different orientations especially of N89, H147, E87 and D177 and their pH-dependent protonation, several hydrogen bonds across the interface can only be formed at acidic but not at

Fig. 4. Alignment of E1 structures solved at different pH values. Stereo-representation of the alignment between the high-resolution structure of E1 solved at pH 5.6 (colored according to Fig. 1) and structures of the individually solved subdomains. The individually solved GFLD at pH 7.5 (PDB ID: 1mwp [23]) is shown in cyan, the CuBD solved at pH 8.0 (PDB ID: 2fjz [25]) is in orange and the CuBD solved at pH 5.4 (PDB ID: 2fk3 [25]) is in purple. Specific hydrogen bonds between atoms are depicted as black broken lines. (a) The loop region between C174 and K178 shows the largest pH-dependent conformational differences. (b) H147 and N89 are rotated in a pH-dependent manner, which leads to the generation of two hydrogen bonds that increase the interaction of both subdomains at acidic pH. In contrast to this, the hydrogen bond between H147 and Y168 is formed within the CuBD only at the higher pH. (c) E87 and D177 face each other directly and form a hydrogen bond only at acidic pH. In the individually solved GFLD and CuBD structures at higher pH, both residues are oriented in opposite directions.

neutral pH. Consequently, the interaction of both subdomains decreases with increasing pH. This was confirmed by mutational studies together with DLS experiments, which showed that exchanging the here identified residues resulted in the loss of strong contacts between the two subdomains constituting E1 at acidic pH and, therefore, a permanently more open conformation of all E1 mutants at both pH values. This pH-dependent interaction explains also why our crystals of the entire E1 were only stably under acidic conditions and dissolved when we attempted to increase the pH beyond ~6.5.

Thus, the E1 domain of APP apparently adopts a more closed conformation in lysosomal vesicles at pH ~5.7 where β -secretase is localized. A more opened conformation is expected to be predominant at the cell surface with a pH of ~7.4 accompanied by an increased apparent molecular weight. Interestingly, previous studies showed a significant effect of the H147N mutation on the proteolytic processing of APP resulting in decreased A β production [33]. This mutant also showed evidence of an altered cellular localization due to decreased post-Golgi trafficking and therefore strongly hints toward the biological importance of the here investigated pH-induced conformational changes and mutations. Our data show that, on the structural level, the H147N mutation impairs the pH-dependent interaction of GFLD and CuBD. Based on these results, we propose a pH sensor within the E1 domain, finally regulating the proteolytic processing of APP. Trafficking of APP to the cell surface and subsequent re-internalization is an essential step for amyloidogenic cleavage of APP by β - and γ -secretase. pH-triggered structural alterations of E1 might directly regulate the interaction of APP to proteins that affect its cellular localization and, therefore, its susceptibility for β -secretase action.

Taken together, the herein investigated amino acid side chains E87, N89, H147 and D177 and the loop segment C174–D177 trigger the tight interaction between GFLD and CuBD at acidic pH. Reducing this interaction could be a highly specific approach to reduce the amyloidogenic processing of APP and hence of medical interest for the treatment of AD.

Materials and Methods

Cloning

The APP-E1 domain without His-tag was cloned, expressed and purified as previously described [19,34]. The four different mutants of E1 were generated from the E1 wt clone [19] by site-directed mutagenesis employing primer pairs corresponding to the following sequence and expressed and purified as the wt protein:

N89A 5'-GTGGTAGAAGCCGCTCAACCAGTGA
CCATC-3'

D177A 5'-GCCCTGCGGAATTGCCAAGTTCCG
CGGGGTAGAGTTTGTG-3'
H147N 5'-GATGTTTGCAGAACTAATCTTCACTGGCA-
CACCGTCGCGAAAGAGACATGC-3'

Success of the mutagenesis was checked by sequencing (Source BioScience LifeSciences).

Crystallization and data collection

Crystals were grown by the sitting-drop vapor diffusion method at 10 °C from 0.1 M Na-citrate (pH 5.6), 20% polyethylene glycol 4000, 11% 2-propanol and 10 mM sarcosine. Therefore, equal volumes of 10 mg/ml protein and reservoir solution were mixed in 24-well plates (MVD/24; Charles Supper). Within 2–3 days, rod-shaped crystals grew to a size of around 500 μ m \times 50 μ m \times 30 μ m. The crystals were transferred to reservoir solution supplemented with 5% *R*(-)-2-methyl-2,4-pentandiol for flash cooling. X-ray data were collected at 100 K and 0.918 Å wavelength at the synchrotron (Helmholtz Zentrum Berlin, BESSY II, BL14.1) [35] up to 1.4 Å resolution (Table 1).

Crystallographic data analysis, structure building and refinement

The crystallographic dataset was processed using the XDSAPP 0.21 software [36,37]. Initially, space group $P6_22$ and after identification of the twin-law $P3_221$ were used for processing. The test set for R_{free} was chosen in thin shells using XDLDATAMAN [38]. The phase problem was solved employing MR with the entire E1 structure (PDB ID: 3ktm [19]) and the program Phaser [39] as implemented in ccp4i 6.3.0 program suite [40]. For MR residues, V47–G50 and C98–H108 were removed from the search model. MR in space group $P3_221$ showed two molecules in the asymmetric unit. Since both pseudotranslation and twinning could result in the apparent presence of an additional symmetry axis, we performed twin analysis with Phenix xtriage [41] and CNS 1.3 [42] and determined the very high twin fraction of 49.7% together with the twin operation $-h, -k, l$. We also analyzed the resolution dependency of quality factors during data reduction in space group $P6_22$ to test for pseudosymmetry, which we could clearly not observe. Next, 40 cycles of manual model building using Coot [43] followed by a twin-based combined positional, twin fraction and *B*-factor refinement using Phenix 1.8.1 [41] and considering NCS restraints (automatic mode) were performed. During this refinement, the missing loop between V47–G50 in both molecules and the loop encompassing the residues C98–C105 in molecule A were completed. Electron density maps were always calculated after detwinning (both CNS 1.3 [42]).

Structure and sequence analysis

PyMOL (DeLano Scientific LLC[†]) was used for rmsd calculation, visualization of molecules and structure comparisons. Electrostatic surface potentials were calculated with APBS [44]. For analysis of interaction interfaces, the PISA server [30] was used. For the calculation of interface areas, the E1 structures were divided into the GFLD (amino

acids 28–120) and the CuBD (amino acids 131–189). For the other used structures of the GFLD (PDB ID: 1mwp) or the CuBD (PDB ID: 2fjz), the same amino acid range was used, except for 2fk3 where only the residues 133–189 were available from the PDB. Searching for structurally similar proteins was performed using PDBeFold provided by the European Bioinformatics Institute [26]. To check for conservation, we generated an alignment using ClustalX 2.1 [45].

Dynamic light scattering

DLS experiments were performed using a DLS 802 instrument (Viskotec) at different protein concentrations. The measurements were performed in 14 μ l and 45 μ l quartz cuvettes (Hellma Analytics) at protein concentration higher and lower than 2.5 mg/ml, respectively. All data were collected at 20 °C with a duration time of 5 s and 50 acquisitions. For the measurements, buffers containing 150 mM NaCl and 5 mM Na_3PO_4 at pH 5.7 and pH 7.4 were used. All measurements were performed in triplicate and the evaluation of the data was performed using the OmniSize software (Viskotec) according to the manufacturer's recommendation. For statistical analysis, a two-tailed, unpaired *t* test was performed using Microsoft Excel. *P* values higher than 0.05 were considered as not significant differences.

Data deposition

The atomic coordinates and structure factors have been deposited in the Protein Data Bank[‡], under the accession code 4pqw.

Acknowledgments

The authors thank J. A. Nzigou-Mandoukou for initiating the crystallization of His-tag-free APP-E1. We acknowledge the Helmholtz Zentrum Berlin, BESSY II, for provision of synchrotron radiation at beamline BL14.1 and thank the scientific staff for assistance. The work was supported by a grant from the Deutsche Forschungsgemeinschaft (SFB 604 to M.E.T.) and the Graduate School "Leibniz Graduate School on Ageing and Age-Related Diseases" of the Fritz Lipmann Institute (to S.H.).

Author Contributions. S.H., S.O.D. and M.E.T. planned research; S.H., K.O. and S.O.D. performed research; S.H., S.O.D. and M.E.T. analyzed data; S.H. and M.E.T. wrote this manuscript.

Conflict of Interest. The authors declare that they have no conflict of interest.

Appendix A. Supplementary data

Supplementary data to this article can be found online at <http://dx.doi.org/10.1016/j.jmb.2014.12.005>.

Received 13 October 2014;
Received in revised form 9 December 2014;
Accepted 9 December 2014
Available online 17 December 2014

Keywords:

Alzheimer's disease;
pH dependence;
dynamic light scattering;
merohedral twinning;
crystal structure

†www.pymol.org.

‡www.rcsb.org.

Abbreviations used:

APP, amyloid precursor protein; AD, Alzheimer's disease;
DLS, dynamic light scattering; wt, wild type; MR,
molecular replacement.

References

- [1] Blennow K, de Leon MJ, Zetterberg H. Alzheimer's disease. *Lancet* 2006;368:387–403.
- [2] Thinakaran G, Koo EH. Amyloid precursor protein trafficking, processing, and function. *J Biol Chem* 2008;283:29615–9.
- [3] Lichtenthaler SF, Haass C, Steiner H. Regulated intramembrane proteolysis—lessons from amyloid precursor protein processing. *J Neurochem* 2011;117:779–96.
- [4] Milward EA, Papadopoulos R, Fuller SJ, Moir RD, Small D, Beyreuther K, et al. The amyloid protein precursor of Alzheimer's disease is a mediator of the effects of nerve growth factor on neurite outgrowth. *Neuron* 1992;9:129–37.
- [5] Kepp KP. Bioinorganic chemistry of Alzheimer's disease. *Chem Rev* 2012;112:5193–239.
- [6] Dahms SO, Konnig I, Roeser D, Guhrs KH, Mayer MC, Kaden D, et al. Metal binding dictates conformation and function of the amyloid precursor protein (APP) E2 domain. *J Mol Biol* 2012;416:438–52.
- [7] von Rotz RC, Kohli BM, Bosset J, Meier M, Suzuki T, Nitsch RM, et al. The APP intracellular domain forms nuclear multiprotein complexes and regulates the transcription of its own precursor. *J Cell Sci* 2004;117:4435–48.
- [8] Müller T, Concannon CG, Ward MW, Walsh CM, Timicieriu AL, Tribl F, et al. Modulation of gene expression and cytoskeletal dynamics by the amyloid precursor protein intracellular domain (AICD). *Mol Biol Cell* 2007;18:201–10.
- [9] Breen KC, Bruce M, Anderton BH. Beta amyloid precursor protein mediates neuronal cell-cell and cell-surface adhesion. *J Neurosci Res* 1991;28:90–100.
- [10] Soba P, Eggert S, Wagner K, Zentgraf H, Siehl K, Kreger S, et al. Homo- and heterodimerization of APP family members promotes intercellular adhesion. *EMBO J* 2005;24:3624–34.
- [11] Ho A, Sudhof TC. Binding of F-spondin to amyloid-beta precursor protein: a candidate amyloid-beta precursor protein ligand that modulates amyloid-beta precursor protein cleavage. *Proc Natl Acad Sci USA* 2004;101:2548–53.
- [12] Haass C, Kaether C, Thinakaran G, Sisodia S. Trafficking and proteolytic processing of APP. *Cold Spring Harbor Perspect Med* 2012;2:a006270.
- [13] Demareux N. pH homeostasis of cellular organelles. *News Physiol Sci* 2002;17:1–5.

- [14] Bencina M. Illumination of the spatial order of intracellular pH by genetically encoded pH-sensitive sensors. *Sensors* 2013; 13:16736–58.
- [15] Capell A, Meyn L, Fluhrer R, Teplow DB, Walter J, Haass C. Apical sorting of beta-secretase limits amyloid beta-peptide production. *J Biol Chem* 2002;277:5637–43.
- [16] Brannstrom K, Ohman A, Nilsson L, Pihl M, Sandblad L, Olofsson A. The N-terminal region of amyloid beta controls the aggregation rate and fibril stability at low pH through a gain of function mechanism. *J Am Chem Soc* 2014;136:10956–64.
- [17] Geneste A, Guillaume YC, Magy-Bertrand N, Lethier L, Gharbi T, Andre C. The protease activity of transthyretin reverses the effect of pH on the amyloid-beta protein/heparan sulfate proteoglycan interaction: a biochromatographic study. *J Pharm Biomed Anal* 2014;97:88–96.
- [18] Coburger I, Hoefgen S, Than ME. The structural biology of the amyloid precursor protein APP—a complex puzzle reveals its multi-domain architecture. *Biol Chem* 2014;395:485–98.
- [19] Dahms SO, Hoefgen S, Roeser D, Schlott B, Gührs K-H, Than ME. Structure and biochemical analysis of the heparin-induced E1 dimer of the amyloid precursor protein. *Proc Natl Acad Sci* 2010;107:5281–7.
- [20] Wang Y, Ha Y. The X-ray structure of an antiparallel dimer of the human amyloid precursor protein E2 domain. *Mol Cell* 2004;15:343–53.
- [21] Keil C, Huber R, Bode W, Than ME. Cloning, expression, crystallization and initial crystallographic analysis of the C-terminal domain of the amyloid precursor protein APP. *Acta Crystallogr Sect D Biol Crystallogr* 2004;60:1614–7.
- [22] Coburger I, Dahms SO, Roeser D, Gührs K-H, Than ME. The overall structure of the multi-domain amyloid precursor protein (APP). *PLoS One* 2013;8:e81926.
- [23] Rossjohn J, Cappai R, Feil SC, Henry A, McKinstry WJ, Galatis D, et al. Crystal structure of the N-terminal, growth factor-like domain of Alzheimer amyloid precursor protein. *Nat Struct Biol* 1999;6:327–31.
- [24] Barnham KJ, McKinstry WJ, Multhaup G, Galatis D, Morton CJ, Curtain CC, et al. Structure of the Alzheimer's disease amyloid precursor protein copper binding domain. *J Biol Chem* 2003;278:17401–7.
- [25] Kong GK-W, Adams JJ, Harris HH, Boas JF, Curtain CC, Galatis D, et al. Structural studies of the Alzheimer's amyloid precursor protein copper-binding domain reveal how it binds copper ions. *J Mol Biol* 2007;367:148–61.
- [26] Krissinel E, Henrick K. Secondary-structure matching (SSM), a new tool for fast protein structure alignment in three dimensions. *Acta Crystallogr Sect D Biol Crystallogr* 2004;60:2256–68.
- [27] Kong GK, Adams JJ, Cappai R, Parker MW. Structure of Alzheimer's disease amyloid precursor protein copper-binding domain at atomic resolution. *Acta Crystallogr Sect F Struct Biol Cryst Commun* 2007;63:819–24.
- [28] Leong SL, Young TR, Barnham KJ, Wedd AG, Hinds MG, Xiao Z, et al. Quantification of copper binding to amyloid precursor protein domain 2 and its *Caenorhabditis elegans* ortholog. Implications for biological function. *Metallomics* 2013;6:105–16.
- [29] Hoefgen S, Coburger I, Roeser D, Schaub Y, Dahms SO, Than ME. Heparin induced dimerization of APP is primarily mediated by E1 and regulated by its acidic domain. *J Struct Biol* 2014;187:30–7.
- [30] Krissinel E, Henrick K. Inference of macromolecular assemblies from crystalline state. *J Mol Biol* 2007;372:774–97.
- [31] Kaden D, Munter L-M, Joshi M, Treiber C, Weise C, Bethge T, et al. Homophilic interactions of the amyloid precursor protein (APP) ectodomain are regulated by the loop region and affect γ -secretase cleavage of APP. *J Biol Chem* 2008; 283:7271–9.
- [32] Andersen JF, Sanders DA, Gasdaska JR, Weichsel A, Powis G, Montfort WR. Human thioredoxin homodimers: regulation by pH, role of aspartate 60, and crystal structure of the aspartate 60 \rightarrow asparagine mutant. *Biochemistry* 1997;36: 13979–88.
- [33] Spoerri L, Vella LJ, Pham CL, Barnham KJ, Cappai R. The amyloid precursor protein copper binding domain histidine residues 149 and 151 mediate APP stability and metabolism. *J Biol Chem* 2012;287:26840–53.
- [34] Honarmand Ebrahimi K, Dienemann C, Hoefgen S, Than ME, Hagedoorn P-L, Hagen WR. The amyloid precursor protein (APP) does not have a ferroxidase site in its E2 domain. *PLoS One* 2013;8:e72177.
- [35] Mueller U, Darowski N, Fuchs MR, Forster R, Hellmig M, Paithankar KS, et al. Facilities for macromolecular crystallography at the Helmholtz-Zentrum Berlin. *J Synchrotron Radiat* 2012;19:442–9.
- [36] Krug M, Weiss MS, Heinemann U, Mueller U. XDSAPP: a graphical user interface for the convenient processing of diffraction data using XDS. *J Appl Crystallogr* 2012;45: 568–72.
- [37] Kabsch W. XDS. *Acta Crystallogr Sect D Biol Crystallogr* 2010;66:125–32.
- [38] Kleywegt GJ, Jones TA. xDIMPAN and xDATAMAN—programs for reformatting, analysis and manipulation of biomacromolecular electron-density maps and reflection data sets. *Acta Crystallogr Sect D Biol Crystallogr* 1996;52: 826–8.
- [39] McCoy AJ, Grosse-Kunstleve RW, Adams PD, Winn MD, Storoni LC, Read RJ. Phaser crystallographic software. *J Appl Crystallogr* 2007;40:658–74.
- [40] Potterton E, Briggs P, Turkenburg M, Dodson E. A graphical user interface to the CCP4 program suite. *Acta Crystallogr Sect D Biol Crystallogr* 2003;59:1131–7.
- [41] Adams PD, Afonine PV, Bunkoczi G, Chen VB, Davis IW, Echols N, et al. PHENIX: a comprehensive Python-based system for macromolecular structure solution. *Acta Crystallogr Sect D Biol Crystallogr* 2010;66:213–21.
- [42] Brunger AT. Version 1.2 of the crystallography and NMR system. *Nat Protoc* 2007;2:2728–33.
- [43] Emsley P, Cowtan K. Coot: model-building tools for molecular graphics. *Acta Crystallogr Sect D Biol Crystallogr* 2004;60:2126–32.
- [44] Baker NA, Sept D, Joseph S, Holst MJ, McCammon JA. Electrostatics of nanosystems: application to microtubules and the ribosome. *Proc Natl Acad Sci USA* 2001;98: 10037–41.
- [45] Larkin MA, Blackshields G, Brown NP, Chenna R, McGettigan PA, McWilliam H, et al. Clustal W and Clustal X version 2.0. *Bioinformatics* 2007;23:2947–8.